© 2020. Published by The Company of Biologists Ltd | Journal of Cell Science (2020) 133, jcs239681. doi:10.1242/jcs.239681

RESEARCH ARTICLE

Frustration of endocytosis potentiates compression-induced receptor signaling

Francesco Baschieri*,‡, Dahiana Le Devedec*, Samuel Tettarasar, Nadia Elkhatib and Guillaume Montagnac‡

ABSTRACT

Cells experience mechanical stresses in different physiological and pathological settings. Clathrin-coated structures (CCSs) are sensitive to such perturbations in a way that often results in a mechanical impairment of endocytic budding. Compressive stress is a mechanical perturbation that leads to increased membrane tension and promotes proliferative signals. Here, we report that compression leads to frustration of CCSs and that CCSs are required to potentiate receptor-mediated signaling in these conditions. We show that cell compression stalled CCS dynamics and slowed down the dynamic exchange of CCS components. As previously reported, compression-induced paracrine activation of the epidermal growth factor receptor (EGFR) was the primary cause of ERK (ERK1 and ERK2, also known as MAPK3 and MAPK1, respectively) activation in these conditions. We observed that EGFR was efficiently recruited at CCSs upon compression and that CCSs were required for full ERK activation. In addition, we demonstrated that compression-induced frustrated CCSs could also increase ligand-dependent signaling of other receptors. We thus propose that CCS frustration resulting from mechanical perturbations can potentiate signaling through different receptors, with potential important consequences for the adaptation of the cell to its environment.

This article has an associated First Person interview with the first author of the paper.

KEY WORDS: Clathrin, Endocytosis, Signaling

INTRODUCTION

Clathrin-mediated endocytosis (CME) relies on the assembly of clathrin-coated structures (CCSs) at the internal leaflet of the plasma membrane. CCSs are endowed with the capacity to recruit specific receptors and to bend the membrane in order to generate receptor-containing endocytic vesicles (McMahon and Boucrot, 2011). Membrane bending is, however, sensitive to mechanical perturbations that oppose the invagination force generated by CCSs. For instance, high plasma membrane tension stalls CCS invagination and thus prevents CME (Boulant et al., 2011; Raucher and Sheetz, 1999). Other types of mechanical perturbations can also prevent normal CCS budding. For example, a subset of CCSs termed tubular clathrin/AP-2 lattices (TCALs), which specifically nucleate at contact sites between the cell and collagen fibers, show reduced dynamics because they attempt, and fail, to internalize fibers that are longer than the cell itself (Elkhatib et al., 2017). High substrate rigidity can also impair CCS budding through favoring the αvβ5-integrin-dependent formation of flat and long-lived clathrin-coated plaques (Baschieri et al., 2018). Thus, CCS frustration is a common response to a wide array of mechanical perturbations. CCS frustration might not simply be a passive consequence of environmental perturbations but could actually participate in building an adapted response to these modifications. Indeed, we showed that TCALs help the cell to migrate in 3D environments (Elkhatib et al., 2017) and that clathrin-coated plaques that assemble on stiff substrates serve as signaling platforms for different receptors, ultimately leading to sustained cell proliferation (Baschieri et al., 2018).

Cell compression was recently shown to induce CCS frustration as well, most likely because of an increased membrane tension (Ferguson et al., 2017). Compressive forces are frequently encountered in the organism, whether in a physiological or pathological context (Butcher et al., 2009; Kalli and Stylianopoulos, 2018; Nia et al., 2017; Rakesh et al., 2010; Tschumperlin et al., 2004). These forces deeply impact the cell physiology and modulate signaling pathways as well as gene expression profile. For example, in bronchial epithelial cells, compression has been shown to activate the epidermal growth factor receptor (EGFR) through a force-induced, metalloprotease-dependent shedding of heparin-binding EGF (HB-EGF) precursor (Tschumperlin et al., 2004). In addition, mechanical compression in solid tumors was reported to promote both proliferation and apoptosis via mechanisms that are still not entirely clear (Alessandri et al., 2013; Cheng et al., 2009). Yet, whether compression-induced EGFR activation (Tschumperlin et al., 2002, 2004) occurs in tumors is not known. Because we previously observed that EGFR uses frustrated clathrin-coated plaques as signaling platforms (Baschieri et al., 2018), we wondered whether pressure-induced CCS frustration could participate in EGFR signaling in these conditions.

RESULTS

Compression reduces CCS dynamics

To investigate the consequences of compressive forces on CCS dynamics, we used HeLa cells that were genome-edited to express a fluorescently-tagged version of μ2-adaptin (AP2M1), a subunit of the clathrin adaptor AP-2 (Fig. S1A–C). Cells were grown on glass coverslips and confined under an agarose plug under a constant compressive stress of 1 kPa (see Materials and Methods; Fig. S1D) that closely match the reported stress observed in solid tumors (0.21–20 kPa in tumors; negligible in healthy tissues) (Fernández-Sánchez et al., 2015; Kalli and Stylianopoulos, 2018; Nia et al., 2017). We noticed that confinement induced an enlargement of the cell area, and blebs were often observed at the cell edges (Fig. S1E), suggesting that membrane tension is most likely dramatically increased in these conditions (Gauthier et al., 2012). In addition, the nuclei of cells under compression were enlarged and nuclear blebs were also visible at their rim (Fig. S1F). These observations indicate that cells are indeed experiencing compression in our assays.

Inserm U1279, Gustave Roussy Institute, Université Paris-Saclay, 94805 Villejuif, France.
*These authors contributed equally to this work

‡Authors for correspondence (guillaume.montagnac@gustaveroussy.fr; francesco.baschieri@gustaveroussy.fr)

F.B., 0000-0003-0218-5320; G.M., 0000-0001-7999-819X

Handling Editor: Andrew Ewald
Received 26 September 2019; Accepted 28 July 2020

Journal of Cell Science

Journal of Cell Science (2020) 133, jcs239681. doi:10.1242/jcs.239681

Because compression stress higher than 3.87 kPa has been reported to increase apoptosis in tumor spheroids *in vitro* (Cheng et al., 2009), we tested whether a transient solid stress of 1 kPa could modulate apoptosis or proliferation rates and found no significant differences between control cells and cells that experienced compression (Fig. S1G,H). In classical culture conditions, HeLa cells display a mixture of dynamic, diffraction-limited CCSs, corresponding to canonical clathrin-coated pits, and long-lived, large CCSs, corresponding to clathrin-coated plaques. We observed that compression globally increased the lifetime of CCSs as well as the occurrence of plaques (as defined by a lifetime greater than 300 s; Fig. 1A,B), thus confirming previous reports (Ferguson et al., 2017). Because integrin αvβ5, which is necessary for clathrin-coated plaque assembly, could possibly play a role in the pressure-induced global increase of CCS lifetime, we treated cells with cilengitide, a potent αvβ5 inhibitor. While CCSs were mostly dynamic in cilengitide-treated cells before pressure, confinement under the agarose gel dramatically increased the lifetime of CCSs as well as the occurrence of stalled CCSs (Fig. 1A,C). These results indicate that the increased lifetime and stabilization of CCSs under compression is independent of αvβ5 integrin and is most likely the consequence of increased membrane tension. Membrane tension was recently shown to regulate the dynamics of CCS components (Bucher et al., 2018). To investigate whether pressure also impacts on the dynamics of major CCS components in our system, we performed fluorescence recovery after photobleaching (FRAP) experiments in cells expressing GFP-tagged μ2-adaptin. We chose to FRAP large and long-lived individual CCSs corresponding to

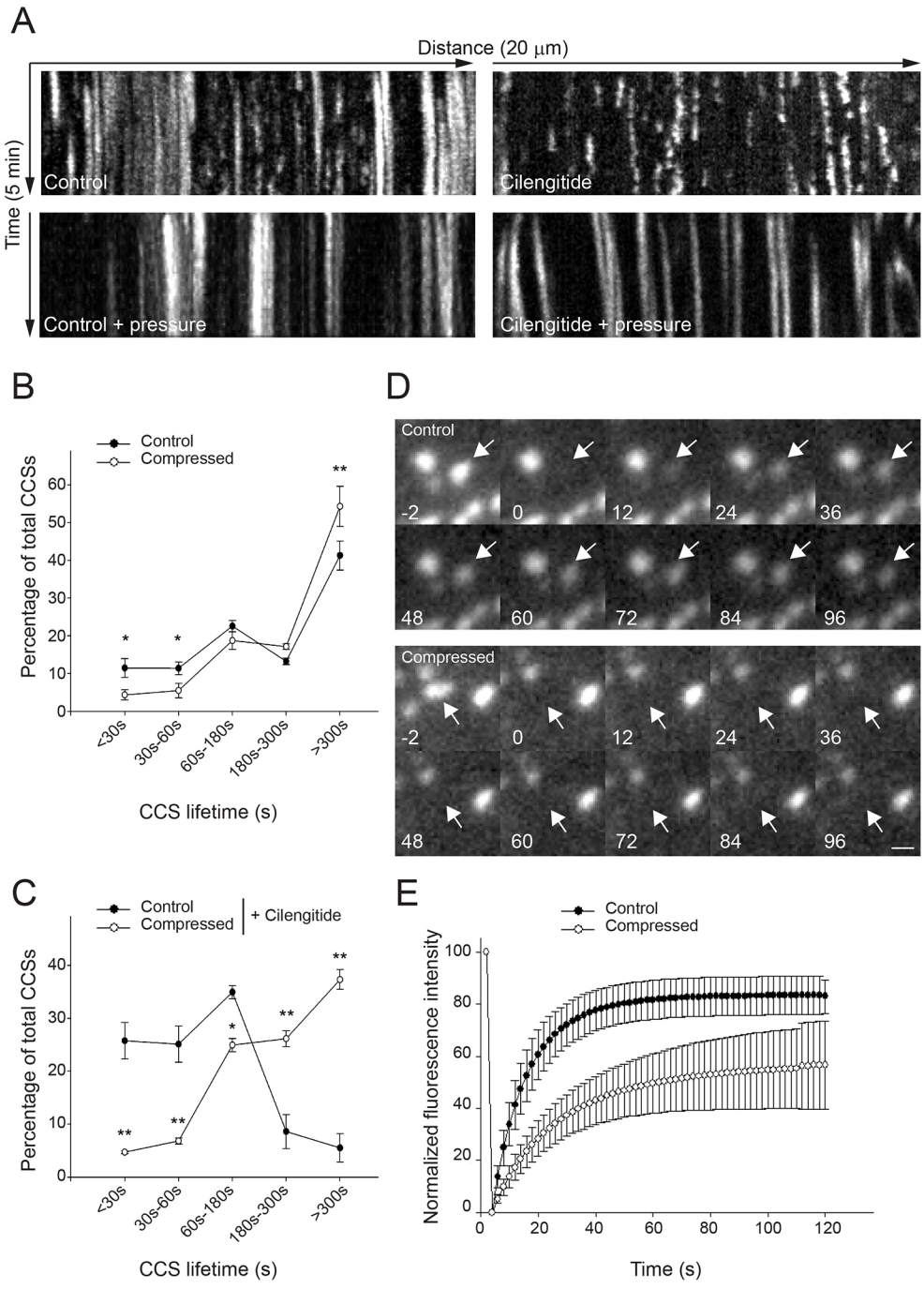

Fig. 1. Cell compression reduces CCS dynamics. (A) Kymographs showing CCS dynamics in genome-edited HeLa cells expressing endogenous mCherry-tagged μ2-adaptin that were either compressed or not under an agarose plug and treated or not with cilengitide, as indicated. Cells were imaged by spinning-disk microscopy every 5 s for 5 min. (B,C) Quantification of the dynamics of CCSs observed as in A. n=3. *P<0.05, **P<0.001, as compared to control condition (one-way ANOVA). (D) Gallery depicting fluorescence recovery of a single CCS (arrows) after photobleaching in control (upper panels) or compressed (lower panels) cells. Time before or after photobleaching is indicated in seconds. Scale bar: 1 μm. (E) Quantification of fluorescence recovery as in D, in control or compressed cells as indicated. All results are expressed as mean±s.d.

Journal of Cell Science (2020) 133, jcs239681. doi:10.1242/jcs.239681

clathrin-coated plaques, because the long-lived nature of these structures allows monitoring of fluorescence recovery over minutes. In control conditions, fluorescence recovery was fast (half time of recovery, $t_{1/2}$≈8 s) with a plateau reaching ∼80%, thus showing that only ∼20% of AP-2 complexes were immobile at CCSs (Fig. 1D,E). However, the mobile fraction only reached ∼60% and the half time of recovery was increased when pressure was applied to cells ($t_{1/2}$≈15 s; Fig. 1D,E). Although we cannot strictly exclude that FRAP parameters may be affected by vesicular budding (Chen et al., 2019), these results suggest that cell compression slows down AP-2 turnover in a similar manner as increased membrane tension (Saleem et al., 2015).

Compression leads to CCS-dependent EGFR signaling

Compressive forces have been reported to activate EGFR and downstream ERK signaling (Tschumperlin et al., 2002, 2004). Indeed, we observed that compression triggered transient activation of ERK (ERK1 and ERK2, also known as MAPK3 and MAPK1,

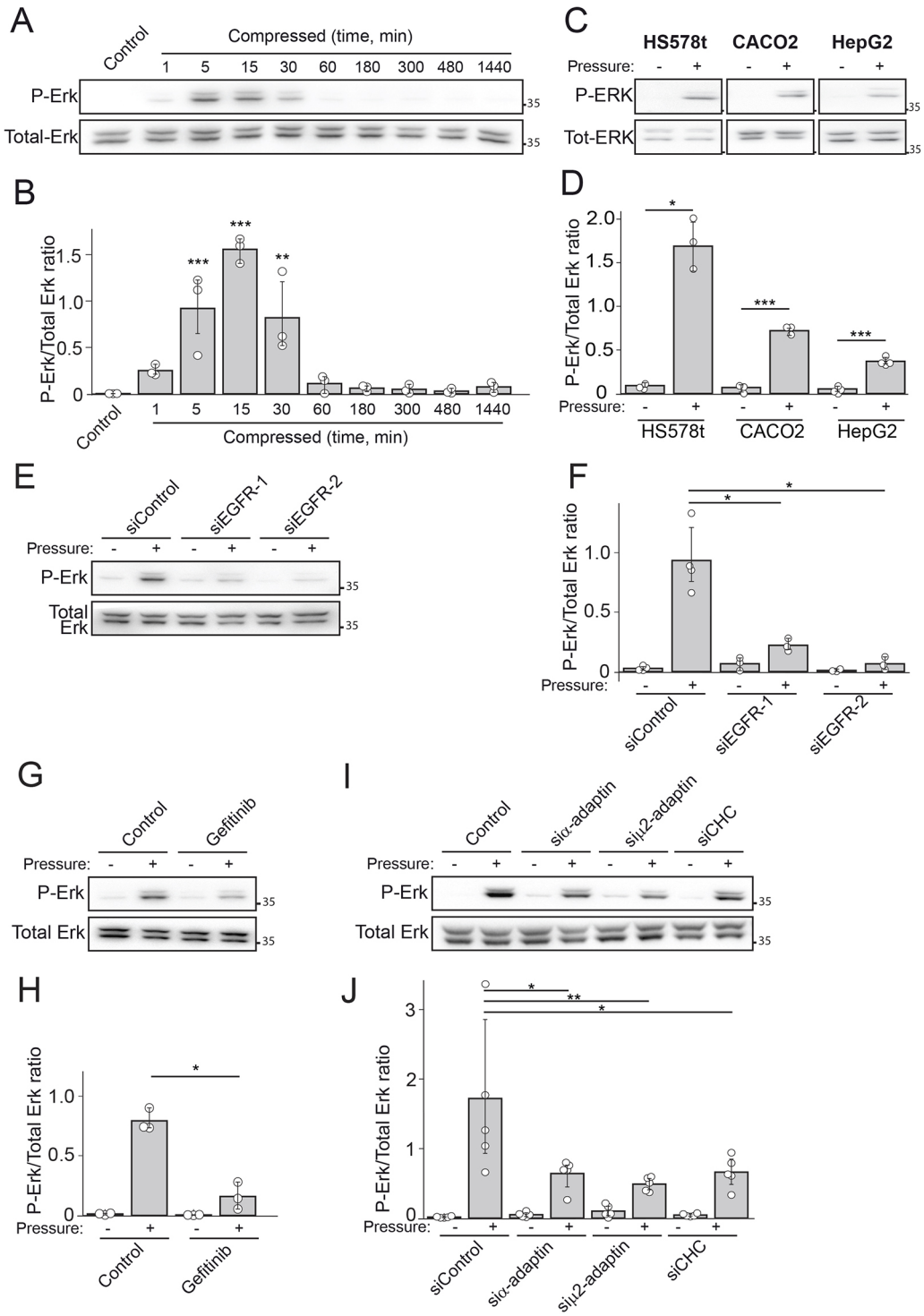

Fig. 2. See next page for legend.

Journal of Cell Science (2020) 133, jcs239681. doi:10.1242/jcs.239681

Fig. 2. CCSs are required for EGFR-dependent signaling. (A) Western blot analysis of phospho-ERK (P-ERK) levels in HeLa cells uncompressed (control) or compressed for different time periods, as indicated (representative image of three independent experiments). Total ERK was used as loading control. (B) Densitometry analysis of bands obtained in western blots as in A. Results are expressed as mean±s.d. ratio of P-ERK:total ERK from three independent experiments. ***P*<0.005, ****P*<0.001 (Kruskal–Wallis one-way ANOVA on ranks). (C) Western blot analysis of P-ERK levels in the indicated cell lines compressed or not for 30 min (representative image of three independent experiments). Total ERK was used as loading control. (D) Densitometry analysis of bands obtained in western blots as in C. Results are expressed as mean±s.d. ratio of P-ERK:total ERK from three independent experiments. **P*<0.05, ****P*<0.001 (two-tailed paired *t*-test). (E) Western blot analysis of P-ERK levels in HeLa cells compressed or not for 30 min and treated or not with EGFR-specific siRNAs, as indicated (representative image of four independent experiments). Total ERK was used as loading control. (F) Densitometry analysis of bands obtained in western blots as in E. Results are expressed as mean±s.d. ratio of P-ERK:total ERK from four independent experiments. **P*<0.05 (one-way ANOVA). (G) Western blot analysis of P-ERK levels in HeLa cells compressed or not for 30 min and treated or not with gefitinib for 1 h prior to compression (representative image of three independent experiments). Total ERK was used as loading control. (H) Densitometry analysis of bands obtained in western blots as in G. Results are expressed as mean±s.d. ratio of P-ERK:total ERK from three independent experiments. **P*<0.05 (one-way ANOVA). (I) Western blot analysis of P-ERK levels in HeLa cells compressed or not for 30 min and treated or not with AP-2 subunits- or CHC-specific siRNAs, as indicated (representative image of five independent experiments). Total ERK was used as loading control. (J) Densitometry analysis of bands obtained in western blots as in I. Results are expressed as mean±s.d. ratio of P-ERK:total ERK from five independent experiments. **P*<0.05, ***P*<0.005 (Kruskal–Wallis one-way ANOVA on ranks). Molecular mass markers in A,C,E,G,I are indicated in kDa.

respectively) (Fig. 2A,B). Similar observations were made in cells experiencing a hypo-osmotic shock, a condition known to increase membrane tension (Fig. S2A,B). Compression of three different transformed cell lines also led to transient ERK activation (Fig. 2C,D). We also observed that GFP-tagged ERK2 transiently translocated from the cytoplasm to the nucleus when HeLa cells were confined under the agarose plug, thus confirming the activated status of ERK in these conditions (Fig. S2C,D). Pressure-induced ERK activation was dependent on EGFR expression (Fig. 2E,F; Fig. S2E) as well as on EGFR kinase activity, because treatment with the EGFR kinase-activity inhibitor gefitinib inhibited ERK phosphorylation under compression (Fig. 2G,H).

CCSs have been shown to act as platforms that potentiate receptor-mediated signaling, particularly in the case of EGFR (Sigismund et al., 2008; Vieira et al., 1996). Modulation of CCS lifetime is an important regulator of receptor signaling output and, for instance, long-lived clathrin-coated plaques are more potent than dynamic clathrin-coated pits in supporting signaling (Baschieri et al., 2018). Because compression stalls CCS dynamics, we reasoned that compression-induced ERK activation could be at least partially due to the increased lifetime of CCSs induced by mechanical stress. Indeed, we observed that AP-2 subunits or clathrin heavy chain (CHC) knockdown reduced ERK activation under compression (Fig. 2I,J; Fig. S2E). Thus, CCSs are required for full EGFR signaling in compressed cells.

Mechanisms of EGFR recruitment at frustrated CCSs under pressure

EGFR is recruited to CCSs upon ligand-induced activation (Rappoport and Simon, 2009). To ascertain whether compressive stress would lead to the same outcome, genome-edited HeLa cells expressing mCherry-tagged endogenous μ2-adaptin and overexpressing GFP-tagged EGFR were compressed under an agarose plug and monitored using total internal reflection fluorescence (TIRF) microscopy. EGFR quickly accumulated at CCSs upon compression (Fig. 3A,B; Movie 1). Increasing membrane tension through applying a hypotonic shock on cells also resulted in EGFR recruitment at CCSs (Fig. S3A,B). We also observed a punctate phospho-tyrosine staining colocalizing with CCSs in cells experiencing compression (Fig. S3C,D). This staining was specifically lost in cells pretreated with gefitinib (Fig. S3C,D) suggesting that activated EGFR is present at CCSs in control cells under compression. Surprisingly, gefitinib did not prevent compression-induced EGFR accumulation at CCSs (Fig. 3B,D; Movie 2). This latter observation is in favor of a previously proposed model whereby ligand-induced EGFR dimerization is required for interaction with the CCS machinery, in a kinase domain activity-independent manner (Wang et al., 2005).

Of note, all these experiments were performed in the absence of serum and of any added EGFR ligands. It has been reported that, in bronchial epithelial cells, the compression resulting from bronchoconstriction induces ADAM metalloprotease-dependent ectodomain shedding from the EGF-family ligand HB-EGF, thus leading to paracrine–autocrine EGFR stimulation (Tschumperlin et al., 2004). Inactivation of these metalloproteases using the large spectrum metalloprotease inhibitor Batimastat was shown to prevent EGFR activation following compressive stress (Tschumperlin et al., 2004). Indeed, we observed that Batimastat reduced both EGFR recruitment at CCSs (Fig. 3B,C; Movie 2) and ERK activation (Fig. 3E,F) upon compression. Conditioned medium from compressed cells was sufficient to activate ERK in serum-starved cells (Fig. S3E,F). However, conditioned medium from compressed cells treated with Batimastat failed to activate ERK (Fig. S3E,F). Of note, Batimastat did not inhibit ERK activation when EGFR was stimulated using externally added EGF (Fig. S3G,H). We hence subjected Batimastat-treated cells to hypotonic swelling to increase their plasma membrane tension and observed that Batimastat treatment prevented EGFR recruitment to CCSs in these conditions (Fig. S3A,B). Taken together, in agreement with the literature, our data suggest that cellular compression leads to metalloprotease-dependent shedding of EGFR ligands, thus resulting in EGFR activation.

Compression-induced frustration of CCSs modulates receptor sorting

Frustration of the endocytic machinery could potentially impact any CCS cargo. We therefore aimed to determine whether other receptors could also be recruited at CCSs upon cell compression. We first analyzed the dynamics of the prototypical CCS cargo transferrin receptor (TfR), which is usually constitutively recruited at CCSs in order to be internalized. Although mCherry-tagged TfR strongly accumulated at CCSs in control cells, it was excluded from CCSs in compressed cells (Fig. 4A,B; Movie 3). This surprising result suggests that compression modulates receptor sorting at CCSs. Given that EGFR accumulates in CCSs of compressed cells, we sought to test whether EGFR and TfR competed for recruitment to CCSs, despite having different sorting motifs (Bonifacino and Traub, 2003). However, TfR was still excluded from CCSs of compressed cells upon EGFR knockdown, showing that no competition exists between these two receptors (Fig. 4B). We also observed a global increase of plasma membrane TfR-associated signal upon compression (Fig. 4C; Movie 3). This most likely reflects the dramatic inhibition of TfR uptake from the cell surface, leading to its accumulation at the plasma membrane. In addition, we observed in FRAP experiments that fluorescence recovery of

Journal of Cell Science (2020) 133, jcs239681. doi:10.1242/jcs.239681

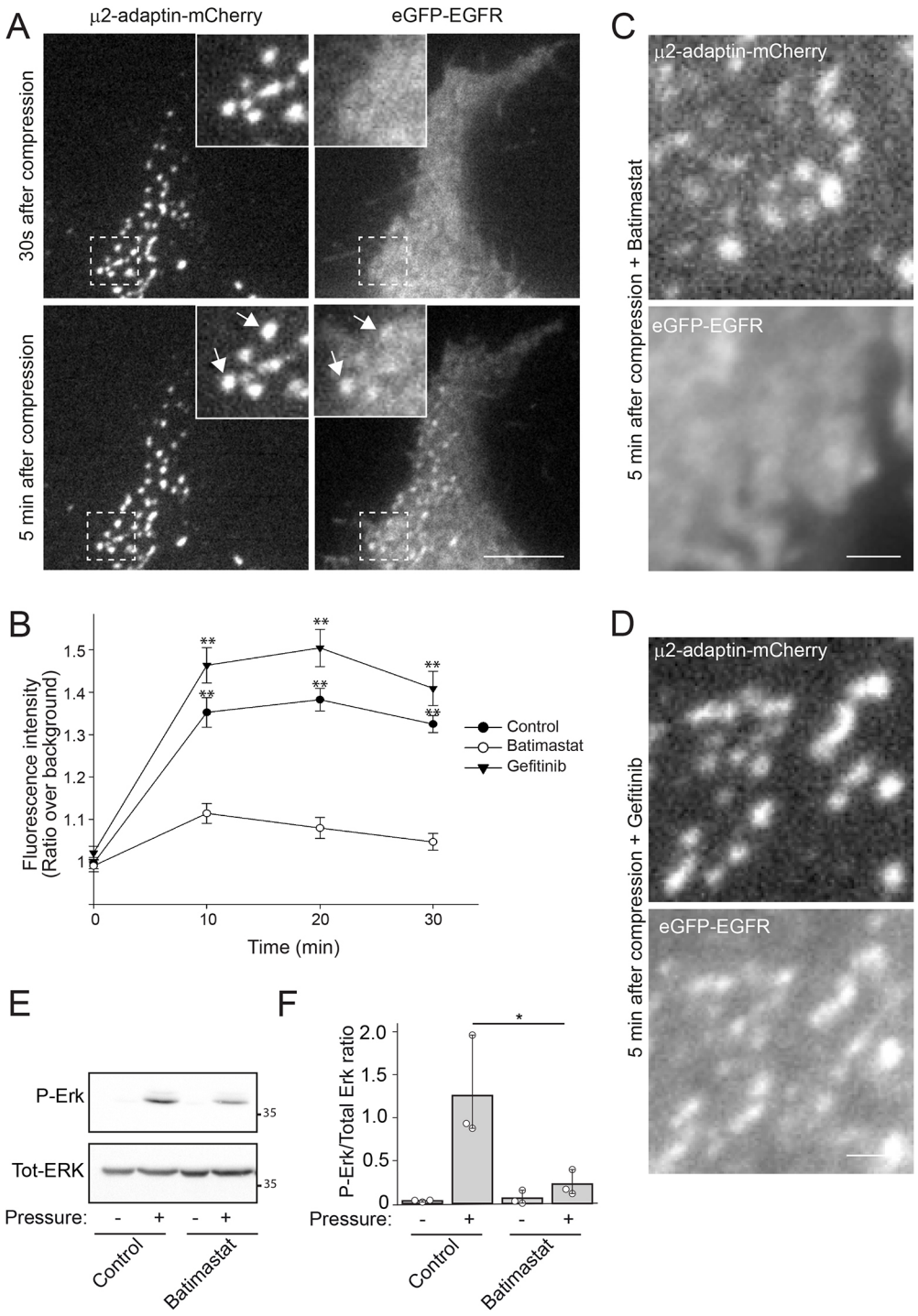

Fig. 3. EGFR is recruited at CCSs under compression. (A) Genome-edited HeLa cells expressing endogenous mCherry-tagged μ2-adaptin were transfected with a plasmid encoding eGFP-tagged EGFR, seeded on glass, compressed under an agarose plug and imaged by TIRF microscopy every 15 s for 30 min. Time after compression is indicated. Higher magnifications of boxed regions are shown. Arrows point to EGFR positive CCSs. Scale bar: 8 μm. (B) Quantification of eGFP–EGFR enrichment at CCSs at the indicated time points after compression in control cells or in cells treated with Batimastat or with gefitinib, as indicated. *n*=3, 20 structures per experiment were analyzed. ***P*<0.001 compared to Batimastat-treated cells (Kruskal–Wallis one-way ANOVA on ranks). (C) Genome-edited HeLa cells expressing endogenous mCherry-tagged μ2-adaptin were transfected with a plasmid encoding eGFP-tagged EGFR and seeded on glass. 24 h later, cells were serum starved for 2 h, treated with 10 μM Batimastat for 1 h, then compressed under an agarose plug and imaged by TIRF microscopy every 15 s for 30 min. Time after compression is indicated. Scale bar: 1 μm. (D) Genome-edited HeLa cells expressing endogenous mCherry-tagged μ2-adaptin were transfected with a plasmid encoding eGFP-tagged EGFR and seeded on glass. 24 h later, cells were serum starved for 2 h, treated with gefitinib for 1 h, then compressed under an agarose plug and imaged by TIRF microscopy every 15 s for 30 min. Time after compression is indicated. Scale bar: 1 μm. (E) Western blot analysis of phospho-ERK (P-ERK) levels in HeLa cells serum starved for 2 h, then treated with 10 μM Batimastat for 1 h, and subjected or not to compression, as indicated (representative image of four independent experiments). Total ERK1/2 was used as a loading control. (F) Densitometry analysis of bands obtained in western blots as in E. Results are expressed as mean±s.d. ratio of P-ERK:total ERK from three independent experiments. **P*<0.05 (one-way ANOVA). Molecular mass markers in E are indicated in kDa.

Journal of Cell Science (2020) 133, jcs239681. doi:10.1242/jcs.239681

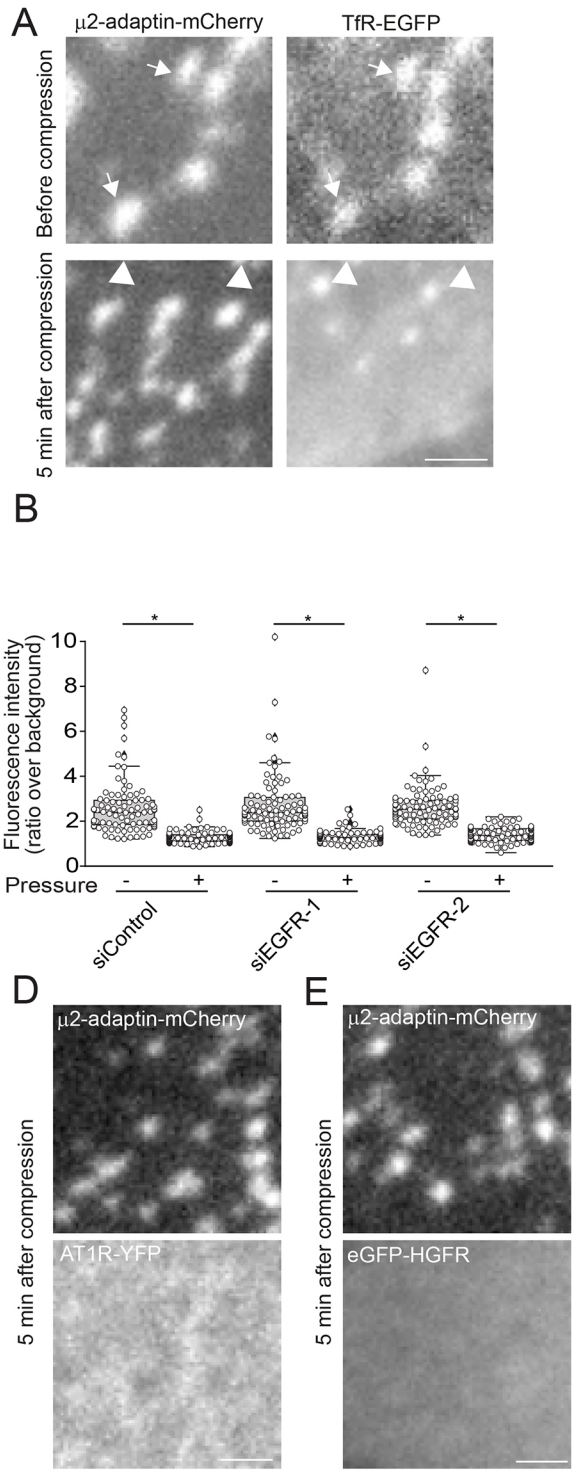

Fig. 4. Receptors are sorted differently in CCSs under compression. (A) Genome-edited HeLa cells expressing endogenous eGFP-tagged μ2-adaptin were transfected with a plasmid encoding mCherry-tagged TfR and were imaged by TIRF microscopy before (upper panel) or 5 min after (lower panel) compression. Arrows point to TfR positive CCSs. Arrowheads point to TfR-positive, AP-2-negative structures most likely corresponding to endosomes. Scale bar: 2 μm. (B) Quantification of mCherry–TfR enrichment at CCSs before or 5 min after compression in cells treated as in A, with the addition of the indicated siRNA treatments. Thirty structures per experiment were analyzed in three independent experiments. **P*<0.05 (Kruskal–Wallis one-way ANOVA on ranks). (C) TfR average intensity at the ventral plasma membrane of HeLa cells as in A was measured before and after compression. Ten cells per experiment were analyzed in three independent experiments. ***P*<0.001 (Wilcoxon test). (D,E) Genome-edited HeLa cells expressing endogenous mCherry-tagged μ2-adaptin were transfected with plasmids encoding YFP-tagged AT1R (D) or GFP-tagged HGFR (E), seeded on glass, compressed under an agarose plug and imaged by TIRF microscopy every 10 s for 30 min. Time after compression is indicated. Scale bars: 1.5 μm. Box plots in B and C indicate the median and 25–75 percentiles, with whiskers showing the boundaries, as assessed using a method that is a function of the interquartile range.

EGFR–GFP at CCSs was reduced in cells experiencing compression, as compared to uncompressed cells stimulated with 10 ng/ml EGF (Fig. S4A). Thus, compression impacts on both CCS component dynamics (Fig. 1D) and CCS cargo dynamics (Fig. 4A,B; Fig. S4A). We next looked at different receptors whose endocytosis is normally triggered by their ligands. The G-protein-coupled receptor (GPCR) angiotensin receptor-1 (AT1R, also known as AGTR1) and hepatocyte growth factor receptor (HGFR, also known as MET), which are recruited at CCSs upon specific ligand stimulation (Fig. S4B,C) (Eichel et al., 2016; Petrelli et al., 2002), did not accumulate at CCSs under pressure in the absence of ligands (Fig. 4D,E). These results indicate that compression does not result in the fast activation of these receptors in the absence of their specific ligands.

Compression-induced frustration of CCSs controls signaling

We reasoned that, beside the specific case of EGFR, frustrated CCSs could have an impact on signaling downstream of other receptors, provided that the ligands of those receptors are present in the system. To test this hypothesis, we incubated HeLa cells in medium supplemented with suboptimal doses of either HGF or angiotensin II and tested the consequences on HGFR or AT1R localization,

Journal of Cell Science (2020) 133, jcs239681. doi:10.1242/jcs.239681

respectively. Neither of the two receptors accumulated at CCSs in these non-acute stimulation conditions (Fig. 5A–D). However, cell compression led to an efficient recruitment of these receptors at CCSs (Fig. 5A–D). Clustering of receptors at CCSs most likely results from low levels of receptor activation, leading to their progressive accumulation at compression-induced frustrated CCSs. In addition, gefitinib-mediated inhibition of EGFR was not sufficient to block ERK activation in compressed cells treated with suboptimal doses of HGF (Fig. 5E,F). This demonstrates that, provided the appropriate ligand is present, receptors other than EGFR can be trapped in compression-induced frustrated CCSs, thus leading to sustained signaling in the ERK pathway.

DISCUSSION

Here, we confirmed previous findings showing that cell compression leads to frustrated endocytosis, with an accumulation of long-lived CCSs (Ferguson et al., 2017). Several pieces of evidence point to a predominant role of integrins in CCS frustration through local anchoring of the CCS machinery to the substrate (Baschieri et al., 2018; De Deyne et al., 1998; Elkhatib et al., 2017).

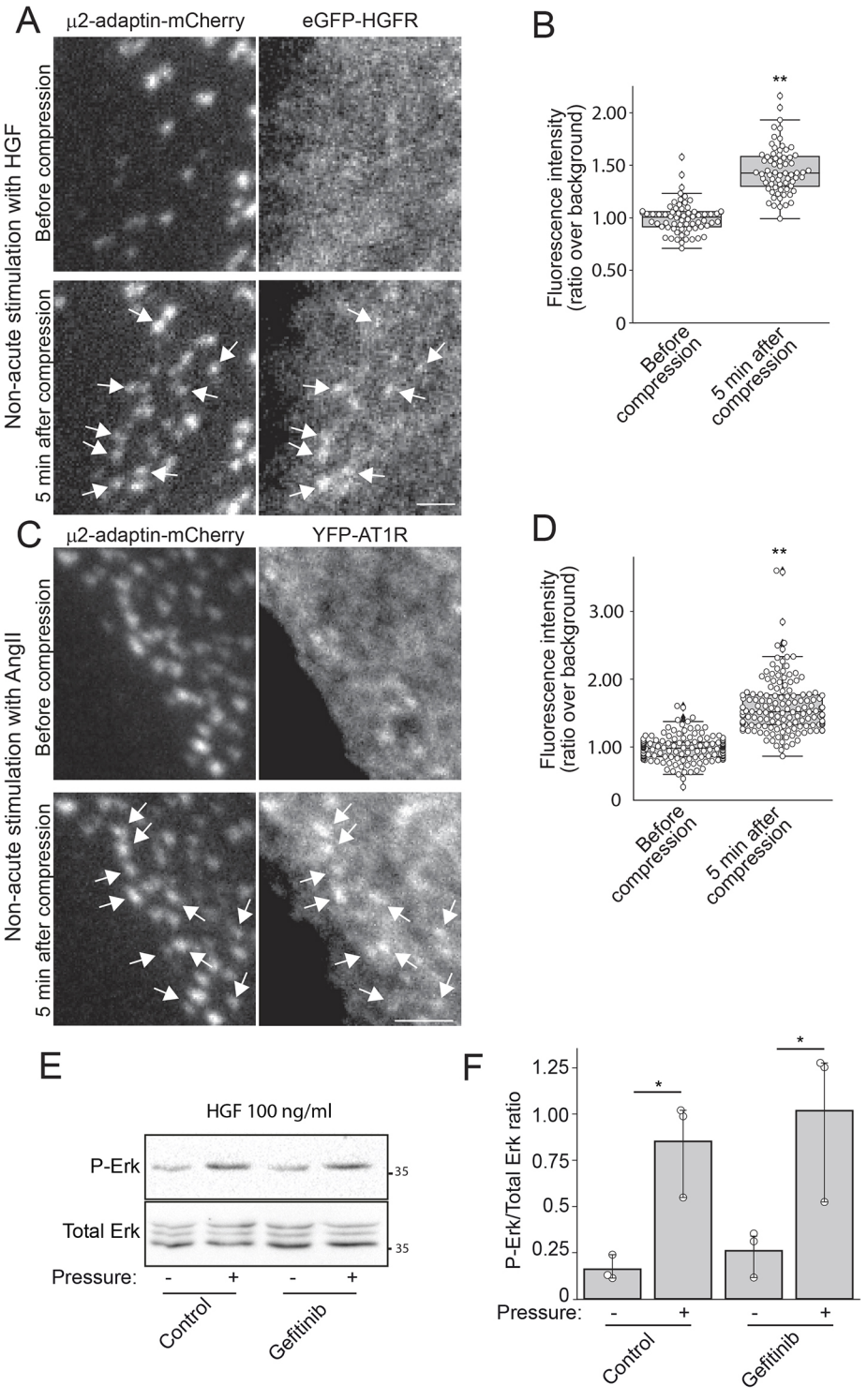

Fig. 5. CCSs under compression can serve as signaling platforms for different receptors. (A) Genome-edited HeLa cells expressing endogenous mCherry-tagged μ2-adaptin were transfected with a plasmid encoding eGFP-tagged HGFR. Cells were seeded on glass and 100 ng/ml HGF was added in the culture medium 1 h before cells were compressed under an agarose plug and imaged by TIRF microscopy every 10 s for 30 min. Time after compression is indicated. Arrows point to HGFR-positive CCSs. Scale bar: 2 μm. (B) Quantification of eGFP–HGFR enrichment at CCSs before or 5 min after compression in control cells treated as in A. At least 20 structures per experiment in three independent experiments were analyzed. $^{**}P<0.001$ (two-tailed paired Student's *t*-test). (C) Genome-edited HeLa cells expressing endogenous mCherry-tagged μ2-adaptin were transfected with a plasmid encoding YFP-tagged AT1R. Cells were seeded on glass and 1 pM angiotensin II was added in the culture medium 5 h before cells were compressed under an agarose plug and imaged by TIRF microscopy every 10 s for 30 min. Time after compression is indicated. Arrows point to AT1R positive CCSs. Scale bar: 2.5 μm. (D) Quantification of YFP–AT1R enrichment at CCSs before or 5 min after compression in control cells treated as in C. Fifty structures per experiment were analyzed in three independent experiments. $^{**}P<0.001$ (two-tailed paired Student's *t*-test). (E) Western blot analysis of phospho-ERK (P-ERK) levels in HeLa cells that were incubated in the presence of HGF for 1 h before being compressed or not and treated or not with gefitinib, as indicated (representative image of three independent experiments). Total ERK was used as a loading control. Molecular mass markers are indicated in kDa. (F) Densitometry analysis of bands obtained in western blots as in E. Results are expressed as mean±s.d. ratio of P-ERK:total ERK from three independent experiments. $^{*}P<0.05$ (one-way ANOVA with Student–Newman–Keuls post hoc test). Box plots in B and D indicate the median and 25–75 percentiles, with whiskers showing the boundaries, as assessed using a method that is a function of the interquartile range.

Journal of Cell Science (2020) 133, jcs239681. doi:10.1242/jcs.239681

HeLa cells display numerous frustrated CCSs, also termed clathrin-coated plaques, whose formation depends on local enrichment of the αvβ5 integrin (Baschieri et al., 2018). Yet, inhibiting this integrin did not prevent the accumulation of long-lived CCSs in cells experiencing compression. Cell compression most likely results in a dramatic increase in membrane tension, which is known to impede CCS budding (Boulant et al., 2011; Raucher and Sheetz, 1999). Thus, our data strongly suggest that frustration of CCSs, as detected in compressed cells, results from increased membrane tension.

We also reported that AP-2 dynamics was perturbed at frustrated CCSs under compression. This might also result from increased membrane tension, because this feature is known to modulate the interaction of CCS components with the plasma membrane (Saleem et al., 2015). Altered dynamics of CCS components is likely to perturb cargo recruitment at CCSs and, indeed, we observed that the TfR was excluded from CCSs under compression. It is not clear why some receptors like EGFR, HGFR, and AT1R could still be recruited at compression-induced frustrated CCSs upon ligand binding, while the TfR, which is normally constitutively addressed to these structures, became excluded. This might depend on the different types of endocytosis motifs present on receptor cytosolic tails that engage different recognition sites on the AP-2 complex and/or on other CCS components (Bonifacino and Traub, 2003). In addition, it remains to be elucidated why the dynamics of EGFR was reduced at compression-induced frustrated CCSs. It is possible that the reduced AP-2 dynamics we observed at frustrated CCSs modulates interactions between cargos and the clathrin coat. Along this line, it was recently shown that clathrin dynamic exchange at CCSs is critical to regulate cargo sorting (Chen et al., 2019).

It was previously reported that EGFR becomes activated in bronchial epithelial cells subjected to mechanical stress, leading to strong ERK activation. This activation has been shown to be dependent on metalloprotease-regulated HB-EGF shedding and on reduction of the intercellular space, leading to paracrine activation of the receptor (Tschumperlin et al., 2004). Our data demonstrate that a similar mechanism exists in different transformed cell lines, suggesting that compression-induced EGFR activation could play an important role in physiopathological situations like solid tumors that are often characterized by high mechanical pressure. Contrary to what was described for bronchial epithelial cells, cancer cells responded to the soluble factor even in non-constricted environments (Fig S3E,F), suggesting that a reduction in intercellular space is dispensable in our model. Surprisingly, we observed that EGFR recruitment at CCSs did not depend on the activity of the kinase domain of the receptor. It has long been believed that EGFR autophosphorylation is required for both signaling output and endocytosis of the receptor (Lamaze and Schmid, 1995). Yet, some studies have suggested that ligand-induced EGFR dimerization is sufficient to induce the accumulation of the receptor at CCSs, without the need for autophosphorylation of the cytosolic tail (Wang et al., 2002, 2005). Our data clearly support this model.

We additionally showed that CCSs are required for full ERK activation downstream of EGFR in compressed cells. These observations are in good agreement with previous reports demonstrating that CCSs can serve as signaling platform for EGFR (Sigismund et al., 2008; Vieira et al., 1996). Yet, we previously demonstrated that clathrin-coated plaques can also serve as signaling platform for other receptors (Baschieri et al., 2018). Here, we report that compression-induced frustrated CCSs could potentiate HGFR signaling when HGF was present in the extracellular environment, leading to strong ERK activation even when EGFR kinase activity was inhibited. It is likely that frustrated CCSs trap the few activated HGFRs that, instead of being internalized, progressively accumulate in these stalled structures. The same holds true for AT1R, raising the possibility that this might be a general mechanism acting to potentiate signaling in cells that experience solid stress. This is of special interest in the case of cancer, where cells are often subjected to mechanical stress in an environment that is rich in several growth factors (Shojaei et al., 2010; Straussman et al., 2012; Zhang et al., 2010).

To conclude, we propose that, in complex microenvironments, mechanical stress leads to activation of the ERK signaling pathway not only because of HB-EGF shedding and paracrine activation of EGFR, but also because compression-induced frustrated CCSs can trap and potentiate signaling by many other receptors.

MATERIALS AND METHODS

Cell lines and constructs

HeLa cells (a gift from Philippe Chavrier, Institut Curie, Paris, France; ATCC CCL-2), genome-edited HeLa cells engineered to expressed an endogenous GFP-tagged or mCherry-tagged μ2-adaptin subunit, HepG2 cells (ATCC HB-8065), Caco-2 cells (ATCC HTB-37) and Hs578t cells (a gift from Christophe Lamaze, Institut Curie, Paris, France), were grown in DMEM Glutamax supplemented with 10% fetal calf serum at 37°C in 5% CO2. For microscopy, cells were serum-starved for at least 2 h before the experiment. All cell lines were tested for mycoplasma contamination. The plasmid encoding GFP–ERK2 was a gift from Dr Hesso Farhan (Institute of Basic Medical Sciences, Oslo, Norway). Plasmids encoding mCherry–TfR (#55144; deposited by Michael Davidson) and EGFR–GFP (#32751; deposited by Alexander Sorkin), and pLenti-MetGFP (#37560; deposited by David Rimm) were from Addgene. The plasmid encoding AT1R–YFP was a kind gift of Dr Mark Scott (Institut Cochin, Paris, France).

Plasmids were transfected 24 h after cell plating using either Lipofectamine 3000 according to the manufacturer's instructions or by electroporating cells in suspension using an AMAXA nucleofector kit V according to the manufacturer's instructions. Alternatively, linear polyethylenimine (PEI; MW 25,000; Polysciences, cat. no. 23966) at 1 mg/ml was used to transfect cells at 50% confluency in a 6-well plate according to the following protocol: 2 μg of DNA was added to 100 μl of OptiMEM, followed by addition of 4 μl of PEI, vortexing and incubation for 10 min at room temperature prior to adding the mix to the cells.

Antibodies and drugs

Rabbit polyclonal anti-total-ERK1/2 (cat. no. 9102) and anti-phospho-ERK1/2 (cat. no. 9101) were purchased from Cell Signaling Technology. Mouse monoclonal anti-total-ERK1/2 (cat. no. 13-6200) was purchased from Thermo Fisher. Mouse monoclonal anti-α-tubulin (cat. no. T9026) was purchased from Sigma. Mouse monoclonal anti-clathrin heavy chain (CHC; cat. no. 610500) and mouse monoclonal anti-Ki-67–FITC (cat. no. 612472) were purchased from BD Biosciences. Mouse monoclonal anti-α-adaptin (cat. no. ab2807), rabbit monoclonal anti-AP2M1 (cat. no. ab75995) and rabbit monoclonal anti-EGFR (cat. no. ab2430) were purchased from Abcam. Rabbit polyclonal anti-α-adaptin antibody (M300) was purchased from Santa Cruz Biotechnology (Santa Cruz, CA, USA). Anti phosphotyrosine (cat. no. 05-321) was obtained from Millipore. AnnexinV–Cy5.5 was from BD Biosciences (cat. no. 559935). Antibodies used for western blot analyses were diluted at 1:1000 in PBS containing 0.1% Tween and either 5% BSA or 5% non-fat dried milk. For immunofluorescence, antibodies were diluted 1:200 in PBS containing 0.3% BSA. Anti-Ki-67–FITC was used at a dilution of 1:500 in PBS containing 0.3% BSA. HRP-conjugated anti-mouse and anti-rabbit antibodies for western blotting were from Jackson ImmunoResearch Laboratories (West Grove, PA, USA) and were used at a dilution of 1:3000. Alexa-conjugated antibodies as well as Cy3- and Cy5-conjugated antibodies were from Molecular Probes (Invitrogen) and were used at a dilution of 1:200. Gefitinib (cat. no.

CDS022106) was purchased from Sigma and used at a final concentration of 10 µM. Cilengitide was purchased from Selleckchem (cat. no. S7077) and used at a final concentration of 10 µM. Human recombinant HGF (cat. no. 1404; used at 100 ng/ml), human recombinant EGF (cat. no. E9644; used at 10 ng/ml), and angiotensin II (cat. no. A9525) were purchased from Sigma. For HGF experiments in Fig 5A and B, cells were previously serum starved for at least 2 h and HGF was added to the serum-free medium for 1 h before the experiment. For AT1R experiments in Fig 5C and D, cells were serum starved for 2 h, then 1pM angiotensin II was added for 5 h in serum-free medium prior to start the experiment. Sir-DNA (Spirochrome; sc-007) was used at 0.5 µM to stain nuclei for live-cell imaging. Cells were incubated for 20 min in the presence of Sir-DNA, then washed once with PBS to eliminate excess Sir-DNA and returned into DMEM.

In vitro compression experiments

To investigate the effect of compressive stress on cell behavior, an under-agarose assay was used (Heit and Kubes, 2003). Cells were plated either in 6-well cell culture plates or in glass-bottom dishes (µ-Dish; cat. no. 190301; Ibidi). 24 h hours later, cells were subjected to mechanical stress using an agarose plug overlaid with the weight necessary to reach a pressure of approximately 1000 Pa (agarose plug of 1.9 cm², corresponding to the area of one well of a 24-well plate, and weight of 20 g). To prepare agarose gels, agar was weighed then dissolved in DMEM Glutamax to a final concentration of 2.4%. The mixture was then cast in an empty dish or well and cooled at room temperature. Agar disks were sterilized under UV light and equilibrated at 37°C before use. For western blotting, cells were subjected to compression for 30 min prior to cell lysis, unless otherwise stated. For video microscopy, videos were started 30 s before applying the compressive stress. Compressed cells were then imaged for 30 min, acquiring one image every 10 s unless stated differently. Alternatively, for CCS dynamics and for FRAP experiments, videos were acquired before and under compression, and the videos before compression were compared to the videos under compression. For ERK2 nuclear enrichment, cells were treated with Sir-DNA, as described above, and imaged by spinning-disk microscopy. Cells were manually segmented in FIJI (https://imagej.net/Fiji), and the Sir-DNA channel was used for the segmentation of the nucleus. Cytoplasm segmentation was obtained by subtracting the area of the nucleus from the cell area. ERK fluorescence was measured over time in the nucleus and in the cytoplasm, then the nuclear enrichment (nuclear:cytosolic signal ratio) was calculated for each cell.

Western blotting

For western blotting experiments, cells were lysed in ice cold MAPK buffer (100 mM NaCl, 10 nM EDTA, 1% IGEPAL CA-630, 0.1% SDS and 50 mM TRIS-HCl pH 7.4) supplemented with protease and phosphatase inhibitors. Protein concentration was measured using a Pierce Coomassie Plus (Bradford) Assay Kit (cat. no. 1856210), according to the manufacturer's instructions, in order to load equal amounts of proteins. Antibodies were diluted at 1:1000 in PBS containing 0.1% Tween and either 5% BSA or 5% non-fat dried milk. For stripping, membranes were incubated in a commercial stripping buffer (cat. no. ST010; Gene Bio-Application) according to the manufacturer's instructions. Western blot quantification was performed in FIJI.

RNA interference

For siRNA depletion, 200,000 cells were plated in 6-well plates. After 24 h, cells were treated with the indicated siRNA (30 nM) using RNAimax (Invitrogen, Carlsbad, CA) according to the manufacturer's instruction. Protein depletion was maximal after 72 h of siRNA treatment, as shown by immunoblotting analysis with specific antibodies. To deplete CHC, α-adaptin or µ2-adaptin, cells were transfected once as described above and then a second time, 48 hours later, with the same siRNAs. In this case, cells were analyzed 96 hours after the first transfection. The following siRNAs were used: µ2-adaptin, 5′-AAGUGGAUGCCUUUCGGGUCA-3′; clathrin heavy chain (CHC), 5′-GCUGGGAAAACUCUUCAGATT-3′; α-adaptin, 5′-AUGGCGGUGGUGUCGGCUCTT-3′; epidermal growth factor receptor (EGFR), 5′-GAGGAAAUAUGUACUACGA-3′ (EGFR-1) and 5′-GCAAAGUGUGUAACGGAAUAGGUAU-3′ (EGFR-2); non-targeting siRNAs (siControl), ON-TARGETplus Non-Targeting SMARTpool siRNAs (Dharmacon D-001810-01). It should be noted that the AP2 complex is stable only when all of its subunits respect a precise stoichiometric ratio and, consequently, depletion of any of the subunits of AP2 leads to loss of all the components of the complex (Boucrot et al., 2010; Motley et al., 2006).

Immunofluorescence microscopy and fluorescence quantification

For anti-phospho-tyrosine staining (P-Tyr), cells were briefly extracted for 30 s using 0.1% Triton prior to fixation in methanol for 10 min. HeLa cells genome edited to express an endogenous GFP-tagged or mCherry-tagged µ2-adaptin subunit were fixed for 2 min in methanol and immunostained. Images were acquired on a Leica Sp8 confocal with a Pecon incubation chamber, equipped with two hybrid and three PMT detectors, using 405, 488, 561 and 633 nm lasers. Imaging was performed using a 63× objective (1.4 NA), if not specified otherwise. Fluorescence of selected regions was measured on at least 50 structures of five different cells per condition in three independent experiments. Data are expressed as mean±s.d. Colocalization between GFP- or mCherry-tagged AP2 and Alexa 568- or Alexa 488-immunostained AP2 was measured using the FIJI plugin JACoP (Bolte and Cordelières, 2006).

Spinning-disk microscopy of live cells

For CCS dynamics, cells were imaged at 5 s intervals for the indicated time using a spinning-disk microscope (Andor) based on a CSU-W1 Yokogawa head mounted on the lateral port of an inverted IX-83 Olympus microscope equipped with a 60×1.35 NA UPLSAPO objective lens and a laser combiner system, which included 491 and 561 nm 30 mW DPSS lasers (Andor). Images were acquired with a Zyla sCMOS camera (Andor). Alternatively, cells were imaged on a Nikon Ti2 Eclipse (Nikon France SAS, Champigny sur Marne, France) inverted microscope equipped with a 60×1.40 NA oil objective (WD 0.130), a sCMOS PRIME 95B camera (Photometrics, AZ, USA) and a dual output laser launch, which included 405, 488, 561 and 642 nm 30 mW lasers. The emission filter characteristics are as follows: 452/45 nm (Semrock Part# FF01-452/45); 470/24 nm (Chroma 348716); 525/50 nm (Semrock Part# FF03-525/50); 545/40 nm (Chroma 346986); 609/54 nm (Semrock Part# FF01-609/54); 708/75 nm (Semrock Part# FF01 708/75). Both microscopes were controlled using Metamorph 7 software (MDS Analytical Technologies, Sunnyvale, CA, USA).

For CCS dynamics quantification, the lifetime of CCSs was measured using the TrackMate plugin of FIJI (Tinevez et al., 2017). Tracks below 5 s in duration (detected in only 1 frame) were discarded. Measured individual lifetimes were pooled into two groups: the 'dynamic' group corresponding to structures with a lifetime below the duration of the movie (5 min) and the 'static' group with a lifetime of 5 min. Of note, the relative percentage of dynamic versus static structures would be dependent on the duration of the movie, because static structures are only counted once whereas dynamic structures continuously nucleate and disappear during the movie. To circumvent this limitation, all quantifications of CCS dynamics represent the relative number of static or dynamic events detectable at the plasma membrane at a given time point. At least 1000 CCSs from at least 5 cells per condition and per experiment were tracked in 3–5 independent experiments. Data are expressed as mean±s.d.

TIRF microscopy and FRAP

For total internal reflection fluorescence microscopy (TIRF), HeLa cells transfected with the indicated plasmids were imaged through a 100×1.49 NA APO TIRF WD 0.13–0.20 oil objective lens on a Nikon Ti2 Eclipse (Nikon France SAS, Champigny sur Marne, France) inverted microscope equipped with a sCMOS PRIME 95B camera (Photometrics, AZ, USA) and a dual output laser launch, which included 405, 488, 561 and 642 nm 30 mW lasers, and driven by Metamorph 7 software (MDS Analytical Technologies, Sunnyvale, CA, USA). A motorized device (Piezo electrical XYZ stage from Nikon) driven by Metamorph allowed the accurate positioning of the illumination light for evanescent wave excitation.

For TIRF–FRAP experiments, one CCS was manually selected and subjected to 100% laser power (30 mW laser) scan in order to have a bleaching of at least 80% of the fluorescence. One frame was collected before photobleaching, and 60 frames were collected after bleaching to analyze fluorescence recovery at a frequency of 1 frame/2 s. The data were analyzed using the FIJI FRAP Profiler plugin (McMaster University, Canada) to extract recovery curves and calculate the half time of recovery.

Apoptosis assays

3×10^5 cells were plated on 6-well plates. 24 h later, compression assays were performed. Cells were trypsinized, resuspended in 1 ml of medium, washed with ice cold PBS, resuspended in binding buffer (0.1 M HEPES, pH 7.4, 1.4 M NaCl and 25 mM $CaCl_2$) at a density of 1×10^6 cells/ml. 1×10^5 cells were then mixed with 5 µl of Annexin-V–Cy5.5 and DAPI (final concentration 1 µg/ml) and incubated at room temperature for 15 min. Then, flow cytometry analysis was performed on a BD FACSAria Fusion. Data were analyzed using FlowJo 10.0.7. Cells positive for Annexin V and negative for DAPI were counted as early apoptotic. Three matched experiments per conditions were performed and data are represented as mean±s.d.

Statistical analyses

Statistical analyses in Fig. 1B,C; Fig. 2F,H; Fig. 3E; Fig. 5F; and Fig. S3H were performed using a one-way ANOVA. Statistical analyses in Fig. 2B,J; Fig. 3B; Fig. 4B; Fig. S1H; Fig. S2B; and Fig. S3B,D,F were performed using a Kruskal–Wallis one-way ANOVA on ranks. Statistical analyses in Fig. 2D; Fig. 5B,D; and Fig. S1G were performed using two-tailed Student's *t*-tests. Statistical analyses in Fig. 4C were performed using the Wilcoxon test. All data are presented as mean±s.d. of at least three independent experiments, except where otherwise stated. Graphics were prepared with the open-source software Instant Clue (Nolte et al., 2018) and statistical analyses were performed using SigmaPlot or Instant Clue software.

Acknowledgements

We thank the imaging facilities of Gustave Roussy for help with image acquisition. Core funding for this work was provided by the Gustave Roussy Institute and Inserm.

Competing interests

The authors declare no competing or financial interests.

Author contributions

Conceptualization: F.B., G.M.; Validation: F.B., N.E.; Investigation: F.B., N.E., D.L.D., S.T.; Formal analysis: F.B.; Writing - original draft preparation: F.B., G.M.; Writing - review & editing: F.B., G.M.; Supervision: G.M.; Funding acquisition: G.M.

Funding

Support was provided by grants from the ATIP–Avenir Program, the Fondation ARC pour la Recherche sur le Cancer, the Groupement des Entreprises Françaises dans la lutte contre le Cancer (GEFLUC) and from the Agence Nationale de la Recherche (ANR-15-CE15-0005-03) to G.M. This project was supported by grant 'Taxe d'apprentissage Gustave Roussy – 2017 – DLD' from the Institut Gustave-Roussy. F.B. acknowledges support by the 2019 Metastasis Award from the Beug Foundation.

Supplementary information

Supplementary information available online at
https://jcs.biologists.org/lookup/doi/10.1242/jcs.239681.supplemental

Peer review history

The peer review history is available online at
https://jcs.biologists.org/lookup/doi/10.1242/jcs.239681.reviewer-comments.pdf

References

Alessandri, K., Sarangi, B. R., Gurchenkov, V. V., Sinha, B., Kiessling, T. R., Fetler, L., Rico, F., Scheuring, S., Lamaze, C., Simon, A., et al. (2013). Cellular capsules as a tool for multicellular spheroid production and for investigating the mechanics of tumor progression in vitro. *Proc. Natl. Acad. Sci. USA* **110**, 14843-14848. doi:10.1073/pnas.1309482110

Baschieri, F., Dayot, S., Elkhatib, N., Ly, N., Capmany, A., Schauer, K., Betz, T., Vignjevic, D. M., Poincloux, R. and Montagnac, G. (2018). Frustrated endocytosis controls contractility-independent mechanotransduction at clathrin-coated structures. *Nat. Commun.* **9**, 3825. doi:10.1038/s41467-018-06367-y

Bolte, S. and Cordelières, F. P. (2006). A guided tour into subcellular colocalization analysis in light microscopy. *J. Microsc.* **224**, 213-232. doi:10.1111/j.1365-2818.2006.01706.x

Bonifacino, J. S. and Traub, L. M. (2003). Signals for sorting of transmembrane proteins to endosomes and lysosomes. *Annu. Rev. Biochem.* **72**, 395-447. doi:10.1146/annurev.biochem.72.121801.161800

Boucrot, E., Saffarian, S., Zhang, R. and Kirchhausen, T. (2010). Roles of AP-2 in clathrin-mediated endocytosis. *PLoS One* **5**, e10597. doi:10.1371/journal.pone.0010597

Boulant, S., Kural, C., Zeeh, J.-C., Ubelmann, F. and Kirchhausen, T. (2011). Actin dynamics counteract membrane tension during clathrin-mediated endocytosis. *Nat. Cell Biol.* **13**, 1124. doi:10.1038/ncb2307

Bucher, D., Mukenhirn, M., Sochacki, K. A., Saharuka, V., Huck, C., Zambarda, C., Taraska, J., Cavalcanti-Adam, E. A. and Boulant, S. (2018). Focal adhesion-generated cues in extracellular matrix regulate cell migration by local induction of clathrin-coated plaques. *bioRxiv* 493114. doi:10.1101/493114

Butcher, D. T., Alliston, T. and Weaver, V. M. (2009). A tense situation: forcing tumour progression. *Nat. Rev. Cancer* **9**, 108-122. doi:10.1038/nrc2544

Chen, Y., Yong, J., Martínez-Sánchez, A., Yang, Y., Wu, Y., De Camilli, P., Fernández-Busnadiego, R. and Wu, M. (2019). Dynamic instability of clathrin assembly provides proofreading control for endocytosis. *J. Cell Biol.* **218**, 3200-3211. doi:10.1083/jcb.201804136

Cheng, G., Tse, J., Jain, R. K. and Munn, L. L. (2009). Micro-environmental mechanical stress controls tumor spheroid size and morphology by suppressing proliferation and inducing apoptosis in cancer cells. *PLoS One* **4**, e4632. doi:10.1371/journal.pone.0004632

De Deyne, P. G., O'Neill, A., Resneck, W. G., Dmytrenko, G. M., Pumplin, D. W. and Bloch, R. J. (1998). The vitronectin receptor associates with clathrin-coated membrane domains via the cytoplasmic domain of its beta5 subunit. *J. Cell Sci.* **111**, 2729-40.

Eichel, K., Jullié, D. and von Zastrow, M. (2016). β-Arrestin drives MAP kinase signalling from clathrin-coated structures after GPCR dissociation. *Nat. Cell Biol.* **18**, 303-310. doi:10.1038/ncb3307

Elkhatib, N., Bresteau, E., Baschieri, F., Rioja, A. L., Van Niel, G., Vassilopoulos, S. and Montagnac, G. (2017). Tubular clathrin/AP-2 lattices pinch collagen fibers to support 3D cell migration. *Science (80-.)* **356**, eaal4713. doi:0.1126/science.aal4713

Ferguson, J. P., Huber, S. D., Willy, N. M., Aygün, E., Goker, S., Atabey, T. and Kural, C. (2017). Mechanoregulation of clathrin-mediated endocytosis. *J. Cell Sci.* **130**, 3631-3636. doi:10.1242/jcs.205930

Fernández-Sánchez, M. E., Barbier, S., Whitehead, J., Béalle, G., Michel, A., Latorre-Ossa, H., Rey, C., Fouassier, L., Claperon, A., Brullé, L., et al. (2015). Mechanical induction of the tumorigenic β-catenin pathway by tumour growth pressure. *Nature* **523**, 92-95. doi:10.1038/nature14329

Gauthier, N. C., Masters, T. A. and Sheetz, M. P. (2012). Mechanical feedback between membrane tension and dynamics. *Trends Cell Biol.* **22**, 527-535. doi:10.1016/j.tcb.2012.07.005

Heit, B. and Kubes, P. (2003). Measuring chemotaxis and chemokinesis: the under-agarose cell migration assay. *Sci. Signal.* **2003**, pl5-pl5. doi:10.1126/stke.2003.170.pl5

Kalli, M. and Stylianopoulos, T. (2018). Defining the role of solid stress and matrix stiffness in cancer cell proliferation and metastasis. *Front. Oncol.* **8**, 55. doi:10.3389/fonc.2018.00055

Lamaze, C. and Schmid, S. L. (1995). Recruitment of epidermal growth factor receptors into coated pits requires their activated tyrosine kinase. *J. Cell Biol.* **129**, 47-54. doi:10.1083/jcb.129.1.47

McMahon, H. T. and Boucrot, E. (2011). Molecular mechanism and physiological functions of clathrin-mediated endocytosis. *Nat. Rev. Mol. Cell Biol.* **12**, 517-533. doi:10.1038/nrm3151

Motley, A. M., Berg, N., Taylor, M. J., Sahlender, D. A., Hirst, J., Owen, D. J. and Robinson, M. S. (2006). Functional analysis of AP-2 α and µ2 subunits. *Mol. Biol. Cell* **17**, 5298-5308. doi:10.1091/mbc.e06-05-0452

Nia, H. T., Liu, H., Seano, G., Datta, M., Jones, D., Rahbari, N., Incio, J., Chauhan, V. P., Jung, K., Martin, J. D., et al. (2017). Solid stress and elastic energy as measures of tumour mechanopathology. *Nat. Biomed. Eng.* **1**, 0004. doi:10.1038/s41551-016-0004

Nolte, H., MacVicar, T. D., Tellkamp, F. and Krüger, M. (2018). Instant clue: a software suite for interactive data visualization and analysis. *Sci. Rep.* **8**, 1–8. doi:10.1038/s41598-018-31154-6

Petrelli, A., Gilestro, G. F., Lanzardo, S., Comoglio, P. M., Migone, N. and Giordano, S. (2002). The endophilin–CIN85–Cbl complex mediates ligand-dependent downregulation of c-Met. *Nature* **416**, 187-190. doi:10.1038/416187a

Rakesh, K., Yoo, B., Kim, I.-M., Salazar, N., Kim, K.-S. and Rockman, H. A. (2010). beta-Arrestin-biased agonism of the angiotensin receptor induced by mechanical stress. *Sci. Signal.* **3**, ra46. doi:10.1126/scisignal.2000769

Rappoport, J. Z. and Simon, S. M. (2009). Endocytic trafficking of activated EGFR is AP-2 dependent and occurs through preformed clathrin spots. *J. Cell Sci.* **122**, 1301-1305. doi:10.1242/jcs.040030

Raucher, D. and Sheetz, M. P. (1999). Membrane expansion increases endocytosis rate during mitosis. *J. Cell Biol.* **144**, 497-506. doi:10.1083/jcb.144.3.497

Saleem, M., Morlot, S., Hohendahl, A., Manzi, J., Lenz, M. and Roux, A. (2015). A balance between membrane elasticity and polymerization energy sets the shape of spherical clathrin coats. *Nat. Commun.* **6**, 6249. doi:10.1038/ncomms7249

Shojaei, F., Lee, J. H., Simmons, B. H., Wong, A., Esparza, C. O., Plumlee, P. A., Feng, J., Stewart, A. E., Hu-Lowe, D. D. and Christensen, J. G. (2010). HGF/c-Met acts as an alternative angiogenic pathway in sunitinib-resistant tumors. *Cancer Res.* **70**, 10090-10100. doi:10.1158/0008-5472.CAN-10-0489

Sigismund, S., Argenzio, E., Tosoni, D., Cavallaro, E., Polo, S. and Di Fiore, P. P. (2008). Clathrin-mediated internalization is essential for sustained EGFR signaling but dispensable for degradation. *Dev. Cell* **15**, 209-219. doi:10.1016/j.devcel.2008.06.012

Straussman, R., Morikawa, T., Shee, K., Barzily-Rokni, M., Qian, Z. R., Du, J., Davis, A., Mongare, M. M., Gould, J., Frederick, D. T., et al. (2012). Tumour micro-environment elicits innate resistance to RAF inhibitors through HGF secretion. *Nature* **487**, 500-504. doi:10.1038/nature11183

Tinevez, J.-Y., Perry, N., Schindelin, J., Hoopes, G. M., Reynolds, G. D., Laplantine, E., Bednarek, S. Y., Shorte, S. L. and Eliceiri, K. W. (2017). TrackMate: an open and extensible platform for single-particle tracking. *Methods* **115**, 80-90. doi:10.1016/j.ymeth.2016.09.016

Tschumperlin, D. J., Shively, J. D., Swartz, M. A., Silverman, E. S., Haley, K. J., Raab, G. and Drazen, J. M. (2002). Bronchial epithelial compression regulates MAP kinase signaling and HB-EGF-like growth factor expression. *Am. J. Physiol. Cell. Mol. Physiol.* **282**, L904-L911. doi:10.1152/ajplung.00270.2001

Tschumperlin, D. J., Dai, G., Maly, I. V., Kikuchi, T., Laiho, L. H., McVittie, A. K., Haley, K. J., Lilly, C. M., So, P. T. C., Lauffenburger, D. A., et al. (2004). Mechanotransduction through growth-factor shedding into the extracellular space. *Nature* **429**, 83-86. doi:10.1038/nature02543

Vieira, A. V., Lamaze, C. and Schmid, S. L. (1996). Control of EGF receptor signaling by clathrin-mediated endocytosis. *Science (80-.)* **274**, 2086-2089. doi:10.1126/science.274.5295.2086

Wang, Y., Pennock, S., Chen, X. and Wang, Z. (2002). Endosomal signaling of epidermal growth factor receptor stimulates signal transduction pathways leading to cell survival. *Mol. Cell. Biol.* **22**, 7279-90. doi:10.1128/MCB.22.20.7279-7290.2002

Wang, Q., Villeneuve, G. and Wang, Z. (2005). Control of epidermal growth factor receptor endocytosis by receptor dimerization, rather than receptor kinase activation. *EMBO Rep.* **6**, 942-948. doi:10.1038/sj.embor.7400491

Zhang, X., Nie, D. and Chakrabarty, S. (2010). Growth factors in tumor microenvironment. *Front. Biosci.* **15**, 151–65. doi:10.2741/3612